Roles of Gag-RNA interactions in HIV-1 virus assembly deciphered by single-molecule localization microscopy

Yantao Yang[a], Na Qu[a], Jie Tan[a], Muaz N. Rushdi[a,b], Christopher J. Krueger[a,b], and Antony K. Chen[a,1]

[a]Department of Biomedical Engineering, College of Engineering, Peking University, 100871 Beijing, China; and [b]Wallace H Coulter Department of Biomedical Engineering, Georgia Institute of Technology, Atlanta, GA 30332

Edited by Eric O. Freed, National Cancer Institute, Frederick, MD, and accepted by Editorial Board Member Stephen P. Goff May 18, 2018 (received for review April 4, 2018)

During HIV-1 assembly, the retroviral structural protein Gag forms an immature capsid, containing thousands of Gag molecules, at the plasma membrane (PM). Interactions between Gag nucleocapsid (NC) and viral RNA (vRNA) are thought to drive assembly, but the exact roles of these interactions have remained poorly understood. Since previous studies have shown that Gag dimer- or trimer-forming mutants (Gag_{ZiL}) lacking an NC domain can form immature capsids independent of RNA binding, it is often hypothesized that vRNA drives Gag assembly by inducing Gag to form low-ordered multimers, but is dispensable for subsequent assembly. In this study, we examined the role of vRNA in HIV-1 assembly by characterizing the distribution and mobility of Gag and Gag NC mutants at the PM using photoactivated localization microscopy (PALM) and single-particle tracking PALM (spt-PALM). We showed that both Gag and Gag_{ZiL} assembly involve a similar basic assembly unit, as expected. Unexpectedly, the two proteins underwent different subsequent assembly pathways, with Gag cluster density increasing asymptotically, while Gag_{ZiL} cluster density increased linearly. Additionally, the directed movement of Gag, but not Gag_{ZiL}, was maintained at a constant speed, suggesting that the two proteins experience different external driving forces. Assembly was abolished when Gag was rendered monomeric by NC deletion. Collectively, these results suggest that, beyond inducing Gag to form low-ordered multimer basic assembly units, vRNA is essential in scaffolding and maintaining the stability of the subsequent assembly process. This finding should advance the current understanding of HIV-1 and, potentially, other retroviruses.

Gag protein | viral RNA | HIV-1 assembly | PALM | spt-PALM

During HIV-1 assembly, the viral structural protein Gag recruits viral RNA (vRNA) to the plasma membrane (PM) from a pool of excess cellular RNAs. This is followed by Gag multimerization, in which Gag molecules interact with one another to form high-order multimers to package the vRNA. Selective recruitment of vRNA has been demonstrated to require only a small number of Gag proteins, which by virtue of the zinc finger motifs within the nucleocapsid domain (NC) are capable of binding with high specificity to the psi-element uniquely present in the vRNA (1–6). Gag multimerization, on the other hand, involves thousands of Gag molecules (7) and is thought to involve electrostatic interactions between NC and vRNA regions other than the psi-element (4, 8–10). As a result, in the absence of vRNA, Gag can still assemble upon cellular RNAs, forming immature capsids that can ultimately remodel into virus-like particles (VLPs) that are nearly indistinguishable in appearance from infectious virus particles (9–11).

Despite the growing understanding of the dependence of HIV-1 assembly on electrostatic NC-RNA interactions, how these interactions drive assembly from nascence to completion has remained elusive. DNA oligonucleotides as short as 15 nucleotides in length can trigger Gag-Gag interactions in vitro (12, 13). Since the length of these oligonucleotides is only about twice the size of the NC binding site, it is possible that the primary role of vRNA in driving Gag multimerization is to bridge two Gag molecules to dimerize. Consistent with this idea, cell-based studies showed that cells expressing an NC-mutant Gag construct (Gag harboring a leucine zipper or isoleucine zipper motif in place of NC that allows Gag to dimerize or trimerize without RNA binding) can efficiently produce VLPs (14, 15). Collectively, these findings have led to the notion that NC-RNA interactions are crucial to Gag assembly and that vRNA functions to drive Gag to form low-order multimers (i.e., dimer/trimers) that can then undergo self-oligomerization to form an immature capsid independent of RNA. Alternatively to in vitro and cell lysate-based studies, standard fluorescence-imaging methods have been used to study Gag assembly (16–23), with one study demonstrating a time-dependent increase in the fluorescence intensity of a diffraction-limited spot emitted by an ensemble of Gag molecules around vRNA at the PM over time (20). However, due to the small dimensions of a budding virion (~150 nm in diameter) and the limited spatial resolution (~250 nm) of standard fluorescence microscopy, the nature of Gag and vRNA interaction within the crowded assembly environment still remains unexplored.

To this end, single-molecule localization microscopy (SMLM) techniques, such as photoactivated localization microscopy (PALM), have enabled visualization of structures densely labeled by specific proteins with spatial resolution ~20 nm in various cellular contexts (24, 25). Additionally, when performed

Significance

Single-molecule localization microscopy (SMLM) is useful for deciphering dynamic organizations of structures densely labeled by specific proteins in the cellular context with nanoscopic resolution not attainable by conventional imaging tools. Here we employed SMLM to investigate the mechanism by which the HIV-1 viral RNA (vRNA) mediates the assembly of thousands of Gag proteins into a virus particle at the plasma membrane. In contrast to the general notion that vRNA only triggers Gag assembly and is dispensable for subsequent assembly, we found that vRNA is indispensable throughout assembly, scaffolding the formation of assembly intermediates and maintaining their architectures via balancing of external forces acting on the assembly environment. These previously unidentified features may facilitate understanding of HIV-1 and, potentially, other retroviruses.

Author contributions: A.K.C. designed research; Y.Y. and N.Q. performed research; Y.Y., N.Q., J.T., M.N.R., and C.J.K. analyzed data; and Y.Y., M.N.R., C.J.K., and A.K.C. wrote the paper.

The authors declare no conflict of interest.

This article is a PNAS Direct Submission. E.O.F. is a guest editor invited by the Editorial Board.

[1]To whom correspondence should be addressed. Email: chenak@pku.edu.cn.

This article contains supporting information online at www.pnas.org/lookup/suppl/doi:10.1073/pnas.1805728115/-/DCSupplemental.

Published online June 11, 2018.

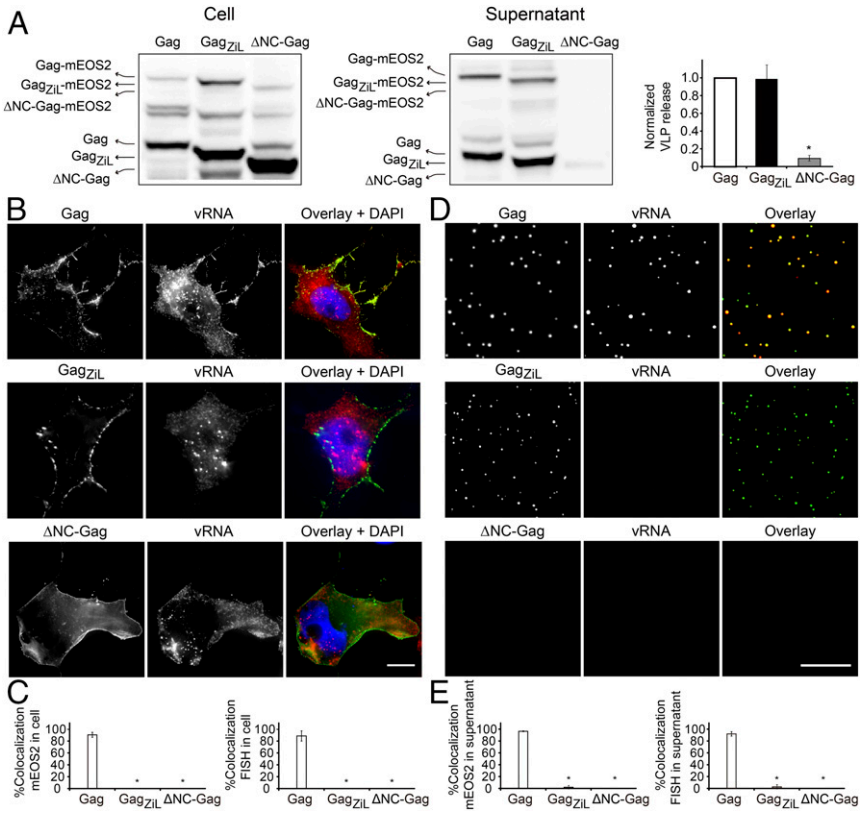

Fig. 1. The effect of mutation in the NC domain on VLP formation and vRNA packaging. COS7 cells were transfected with pNL43ΔPolΔEnv-Gag-mEOS2, pNL43ΔPolΔEnv-ΔNC-Gag-mEOS2, or pNL43ΔPolΔEnv-Gag$_{ZiL}$-mEOS2 (cotransfected with the respective untagged construct in a 1:4 ratio). (*A*) Assessment of virus release efficiency. Western blot was performed with HIV-Ig to detect Gag and Gag-mEOS2 or their NC mutants in supernatant and cells at 24 h posttransfection. Virus release efficiency (*Right*) was calculated as described in *SI Appendix, SI Materials and Methods*, normalized to the level of viral release in cells expressing Gag and Gag-mEOS2. (*B*) Representative images of Gag (detected by mEOS2) and the unspliced HIV-1 viral RNA (detected by FISH) in cells. (*C*) The percentage of mEOS2 signals that were colocalized with FISH signals (percent colocalization mEOS2) and the percentage of FISH signals that were colocalized with mEOS2 signals (percent colocalization FISH) in cells expressing Gag and its NC mutants were calculated on a cell-by-cell basis using a custom MATLAB program. Data represent mean ± SD of at least 15 cells. (*D*) Representative images of Gag or its NC mutants (detected by mEOS2) and unspliced HIV-1 viral RNA (detected by FISH) in virus-like particles released from COS7 cells expressing Gag or its NC mutants. (*E*) Analysis of HIV-1 vRNA packaging efficiency. A custom MATLAB program was written to analyze the percentage of mEOS2-containing particle signals that colocalized with FISH signals (percent colocalization mEOS2) and the percentage of FISH signals that colocalized with mEOS2-containing particle signals (percent colocalization FISH). Data represent mean ± SD of at least 30 independently acquired images for each experimental condition. For *A*, *C*, and *E*, * represents significant difference from Gag ($P < 0.05$). (For *B* and *D*, scale bar, 10 μm.)

in combination with single-particle tracking (spt-PALM), associated protein dynamics within subdiffraction space have been studied (17, 19, 26). In the present work, we sought to decipher the role of NC-RNA interactions in HIV-1 assembly at the PM using PALM and spt-PALM. Specifically, the spatial organization, diffusion, and directed-transport properties were characterized for Gag and for its variants lacking the NC domain, including Gag$_{ZiL}$, an assembly-competent mutant that harbors an isoleucine zipper trimerization motif in place of NC, and ΔNC-Gag, an assembly-deficient mutant that harbors a deletion of NC to render the protein monomeric.

Results

Labeling Gag and NC Mutants with mEOS2. To study HIV-1 assembly by superresolution imaging, the vRNA transcript and its encoded proteins were expressed in COS7 cells by transiently transfecting pNL43 derivative constructs, in which the polymerase (pol) and envelope (env) genes were deleted and Gag was tagged with the photoactivatable fluorescent protein (FP) mEOS2 (i.e., pNL43ΔPolΔEnv-Gag-mEOS2). The pNL43ΔPolΔEnv-Gag-mEOS2 was transfected in a 1:4 ratio with pNL43ΔPolΔEnv-Gag (lacking mEOS2), a transfection condition that can minimize the potential defects in Gag assembly caused by mEOS2 labeling (see *SI Appendix*, Fig. S1 for construct schematics and *SI Appendix*, Fig. S2 for characterization of VLP release in different cell lines). To study the influence of NC on viral assembly, cells expressing ΔNC-Gag-mEOS2 and Gag$_{ZiL}$-mEOS2 in a 1:4 ratio with their corresponding untagged constructs were also prepared (*SI Appendix*, Fig. S1). VLP release efficiency, assayed at 24 h posttransfection of the proviral constructs (*SI Appendix, SI Materials and Methods*), showed VLP production was significantly inhibited in the ΔNC-Gag-mEOS2-expressing cells (Fig. 1*A*), as expected, since deletion of NC attenuates viral production (15, 27). Conversely, VLP release efficiency is fairly similar between the Gag$_{ZiL}$-mEOS2-expressing and the Gag-mEOS2-expressing cells, supporting previous studies showing replacement of NC with an isoleucine zipper can rescue particle assembly (14, 15). Additionally, fluorescence microscopy imaging showed that while all three Gag variants localized at PM (Fig. 1 *B* and *C* and *SI Appendix*, Figs. S3 *B* and *C* and S4), vRNA (assayed by fluorescence in situ hybridization; FISH) colocalized with Gag-mEOS2 but not with ΔNC-Gag-mEOS2 nor Gag$_{ZiL}$-mEOS2, as expected since both ΔNC-Gag and Gag$_{ZiL}$ cannot bind to RNA. Consistent with these results, vRNA was only present in VLPs released by cells expressing Gag but not Gag$_{ZiL}$ or ΔNC-Gag, which formed no particles (Fig. 1 *D* and *E* and *SI Appendix*,

Figs. S3 *D* and *E* and S4). Together, these findings indicate that coexpressing mEOS2-tagged Gag variants with their corresponding untagged Gag variants at a 1:4 ratio could yield similar virus release efficiency and RNA packaging properties as those seen in previous studies, in which only untagged Gag variants were used (14, 15). This establishes mEOS2 as a suitable probe for studying vRNA-mediated Gag assembly by fluorescence imaging.

Nanoscale Organizations of Gag and NC Mutants. Having demonstrated the utility and suitability of mEOS2 for studying HIV-1 assembly, we next sought to study the different Gag variants at the PM using PALM. At 15–18 h posttransfection, COS7 cells were fixed and imaged by PALM. Individual molecules were localized to create PALM images, and their nanoscale organization was determined based on cluster analysis (*SI Appendix*, *SI Materials and Methods*). Since ΔNC-Gag is incapable of particle assembly, while Gag_{ZiL} is capable of particle assembly through RNA-independent isoleucine zipper-mediated trimerization, we hypothesized that these mutants would exhibit different nanoscale organizations from wild-type Gag, which relies on interaction with vRNA to form virus particles at the PM. Hence, comparison of the nanoscale organizations of Gag and the NC mutants should provide insights into the role of NC-RNA interactions during HIV-1 viral assembly.

Gag. Punctate structures, characteristic of assembly complexes or budding viruses, were readily observed across the PM of COS7 cells expressing wild-type Gag (Fig. 2*A*). Cluster analysis revealed that ∼64% of the Gag molecules were associated with clusters with a mean radius of 33.8 ± 0.16 nm (Fig. 2 *B* and *C*), with ∼61% of the clusters having a radius between 20 and 30 nm and very few clusters with radius approaching 150 nm (see *SI Appendix* for more details). Thus, virion formation is likely not driven by delivery to the PM of large and/or late-stage assembly complexes preassembled within the cytoplasm. Rather, it appears to be a multistage process that takes place at the PM, in which Gag forms assembly intermediates of increasing size in a step-wise fashion. Presumably, this process is initiated from an assembly precursor with a radius less than or equal to ∼20 nm, which likely contains a small number of Gag molecules bound to vRNA which may form in the cytoplasm (28). Overall, these findings are consistent with previous biochemical assays showing that Gag assembly is a multistage process (29) and that the PM is the primary site for higher-order Gag multimerization and subsequent particle assembly (4).

Based on in vitro assembly assays, it is thought that Gag continuously becomes more densely clustered during the progression of assembly (13, 30). To investigate this possibility in nanoscale at the PM, Gag cluster density was determined by PALM cluster analysis (*SI Appendix*, *SI Materials and Methods*) (Fig. 2*D*) and was plotted as a function of the cluster radius (Fig. 2*E*). Interestingly, Gag cluster density increased asymptotically with the cluster radius, reaching a plateau at a cluster radius of ∼80 nm. Thus, it appears that HIV-1 assembly is not a process in which Gag molecules interact with each other toward ever more densely packed clusters from nascence to completion, as inferred from in vitro assembly assays. Rather, Gag assembly may involve two distinct growth phases in sequence, separated by a transition in the cluster radius. In the initial phase, Gag molecules are recruited to assembly precursors to form sizable clusters in a manner that favors dense-packing. After the assembly grows to a certain size, the process shifts to a phase in which additional Gag molecules increase cluster size at a constant packing density (Fig. 2*E*). Supporting this idea, a critical cluster radius of ∼63 nm was determined for Gag assembly from a logistic curve-fitting of the cluster density versus cluster radius relationship (*SI Appendix*, Fig. S5).

Gag_{ZiL}. PALM imaging revealed that Gag_{ZiL} formed clusters and exhibited typical viral-budding characteristics similar to wild-type Gag at the PM of COS7 cells (Fig. 2*A*), as expected given that the Gag_{ZiL} mutant is known to be assembly-competent. Approximately 73% of Gag_{ZiL} were found to be associated with clusters, comparable with wild-type Gag clustering (Fig. 2*B*). Despite this similarity, the nanoscale organization of Gag_{ZiL} was quite different from that of Gag. Specifically, Gag_{ZiL} clusters were on average smaller (Fig. 2*C*) and more densely packed than Gag clusters (Fig. 2*D*). Additionally, the density of Gag_{ZiL} clusters increased linearly with cluster radius and did not plateau, as seen in Gag assembly (Fig. 2*F*), and is significantly higher than that of Gag for all cluster radii measured ($P < 0.05$) (Fig. 2*G*). Thus, in contrast to Gag assembly, Gag_{ZiL} appears to assemble through a single, cluster-centric process, in which Gag_{ZiL} trimers interact extensively with one another to form growing clusters with cluster density increasing linearly with cluster radius.

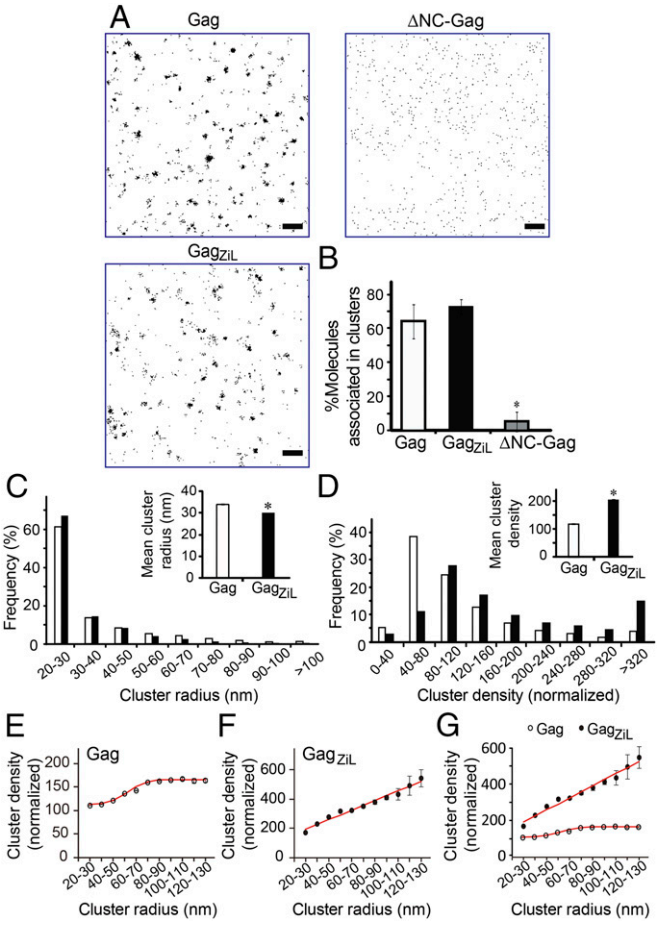

Fig. 2. PALM imaging and cluster formation analysis of Gag and NC mutants. (*A*) Representative PALM images are shown. Individual spots represent single molecules. (Scale bar, 500 nm.) (*B*) Percentage of identified Gag molecules associated with clusters. Values represent mean ± SD determined from at least 11 cells. Cluster information was extracted from PALM images using a Hoshen–Kopelman-based algorithm (*SI Appendix, SI Materials and Methods*). (*C*) Cluster radius distribution of Gag (n = 15,450) and Gag_{ZiL} (n = 14,242). *Inset* shows mean ± SEM radius. (*D*) Cluster-density distribution of Gag (n = 15,450) and Gag_{ZiL} (n = 14,242). For each cell, the cluster densities were normalized with respect to the mean densities across the entire PM. *Inset* shows mean ± SEM density. (*E*) Gag cluster density (from *D*) plotted as a function of cluster radius. The red line represents the least square regression from a logistic curve-fitting (r^2 = 0.98). (*F*) Gag_{ZiL} cluster density (from *D*) plotted as a function of cluster radius. The red line represents the least square linear regression (r^2 = 0.96). (*G*) Gag and Gag_{ZiL} cluster density as a function of cluster radius, plotted together on the same scale. Note that no data were shown for ΔNC-Gag because of its lack of clustering. For *B*, *C*, and *D*, * represents significant difference from Gag ($P < 0.05$).

CELL BIOLOGY

ΔNC-Gag. In contrast to Gag and Gag_{ZiL}, very few clusters were observed at the PM of COS7 cells expressing ΔNC-Gag (Fig. 2*A*). Cluster analysis revealed that ΔNC-Gag molecules did not form clusters (Fig. 2*B*). Thus, lack of NC significantly inhibited Gag's ability to form clusters at the PM. These findings are consistent with the inability of ΔNC-Gag to form VLPs (Fig. 1 and *SI Appendix*, Fig. S3).

Nanoscale Dynamics of Gag and NC Mutants. To further dissect the nature of Gag assembly and its dependence on NC, we studied the mobility of Gag molecules using spt-PALM. At 15–18 h post-transfection of pNL43ΔPolΔEnv-Gag-mEOS2, pNL43ΔPolΔEnv-ΔNC-Gag-mEOS2, or pNL43ΔPolΔEnv-Gag_{ZiL}-mEOS2 (in a 1:4 ratio with the respective untagged construct), spt-PALM imaging was performed at 20 frames per second. After determining the location and the mean square displacement as a function of time lag ($\Delta\tau$) of each molecule with tracks including at least 10 time lags, the lateral molecular diffusion, D_{eff}, and directed-transport properties were analyzed as described in *SI Appendix*, *SI Materials and Methods*.

Gag. Gag was found to exhibit diverse motions at the PM, including stationary, diffusion (Brownian or corralled), and directed transport (Fig. 3*A*). More than 90% of molecules were mobile, with the fraction of mobile molecules undergoing diffusion and directed transport determined to be 92 and 8%, respectively. For the molecules that underwent diffusion, Gag had an overall mean diffusion coefficient of 0.13 ± 0.00 $\mu m^2/s$ (Fig. 3*B*), consistent with previous measurements (19, 26). The diffusing molecules were observed to be equally divided between Brownian and corralled motion (Fig. 3*C*). Of the molecules in directed transport, the mean speed was measured to be 1.35 ± 0.05 μm/s (Fig. 3*D*), which is within the range of measurements previously made for membrane-bound proteins (31–33). Furthermore, the molecules had a mean track acceleration of 0.03 ± 0.05 $\mu m/s^2$, which is not significantly different from zero acceleration ($P = 0.60$, two-tailed t test assuming equal variance) (Fig. 3*E*). Together, these findings suggest Gag assembly through NC-RNA interactions is regulated kinetically by both diffusion and active transport at a constant speed.

Gag_{ZiL}. As seen in cells expressing Gag, Gag_{ZiL} also exhibits a wide range of motions. Eighty-four percent of the Gag_{ZiL} molecules were found to be mobile, with 89 and 11% of the mobile molecules undergoing diffusion and directed motion, respectively. The mean diffusion coefficient of Gag_{ZiL} molecules was 0.09 ± 0.00 $\mu m^2/s$, which was significantly slower than Gag (Fig. 3*B*). Nearly 40 and 60% of the diffusive molecules were Brownian and corralled, respectively (Fig. 3*C*). Thus, it appears that Gag_{ZiL}'s diffusion at the PM is more confined compared with Gag. Of the molecules in directed transport, the mean speed was 0.79 ± 0.04 μm/s, which was significantly lower than the mean speed of Gag (Fig. 3*D*). Notably, Gag_{ZiL} has a mean track acceleration of –0.46 ± 0.04 $\mu m/s^2$ (Fig. 3*E*). This suggests that Gag_{ZiL} molecules experienced a negative driving force to restrict their movement. Together, these results indicate that Gag_{ZiL} on average exhibits slower dynamic properties than Gag. This suggests the mobility of Gag_{ZiL} at the PM is highly restricted and is in good agreement with its propensity to form densely packed clusters, as revealed by our PALM cluster analysis (Fig. 2).

ΔNC-Gag. In contrast to Gag and Gag_{ZiL}, nearly all of ΔNC-Gag were mobile (>99%). The diffusive and directed-transport fractions were 56 and 44%, respectively. Compared with Gag and Gag_{ZiL}, ΔNC-Gag showed more rapid diffusion, with a mean coefficient of diffusion of 0.31 ± 0.01 $\mu m^2/s$ (Fig. 3*B*). Among the diffusing molecules, 91% showed Brownian motion, and 9% showed corralled motion (Fig. 3*C*). Additionally, more than 82% of ΔNC-Gag molecules had diffusion coefficients greater than the mean diffusions of Gag (0.13 $\mu m/s^2$) and Gag_{ZiL} (0.09 $\mu m^2/s$). Of the molecules that traveled by directed transport, the mean speed and mean acceleration were 1.79 ± 0.06 μm/s (Fig. 3*D*) and 0.14 ± 0.08 $\mu m/s^2$ (Fig. 3*E*), respectively. Thus, compared with Gag and Gag_{ZiL}, ΔNC-Gag exhibits higher mobility at the PM, suggesting its movement is less constrained. This is consistent with its inability to undergo viral RNA-mediated cluster assembly and viral budding (Fig. 1 and *SI Appendix*, Fig. S3).

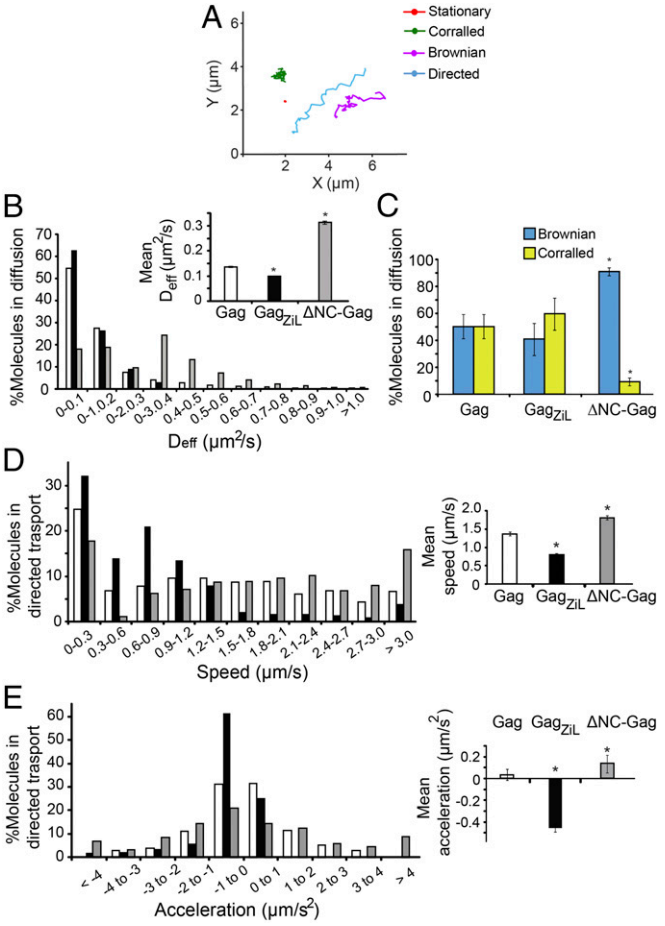

Fig. 3. Dynamics of Gag and NC mutants at the PM, assessed by spt-PALM. (*A*) Representative full-track movements of Gag at the PM. Gag exhibits a wide range of motions including no movement, diffusion (Brownian or corralled), and directed transport. (*B*) Analysis of lateral diffusion. The histogram shows the distribution of diffusion coefficients of single complexes of Gag and NC mutants. Total tracks of Gag (n = 3,604), Gag_{ZiL} (n = 1,730), and ΔNC-Gag (n = 1,115) were acquired from at least 11 cells. *Inset* shows mean ± SEM diffusion coefficients. (*C*) Plot of the percentage of molecules showing either Brownian (blue bar) or corralled (yellow bar) diffusion of Gag and its NC mutants at the cellular PM. Data represent mean ± SD of at least 11 cells. (*D*) Analysis of directed-transport properties of Gag and NC mutants. The histogram shows the distribution of the speed of single trajectories acquired for Gag and NC mutants. *Right* shows mean ± SEM speed. (*E*) The histogram shows the distribution of the mean acceleration of single trajectories acquired for Gag and NC mutants. *Right* shows mean ± SEM acceleration. For *D* and *E*, total tracks of Gag (n = 598), Gag_{ZiL} (n = 430), and ΔNC-Gag (n = 519). * represents significant difference from Gag ($P < 0.05$).

Discussion

Nucleocapsid (NC) is the major RNA-binding domain that enables vRNA-mediated assembly of Gag monomers into HIV-1 virus in the complex membrane environment. The mechanism underlying this dependence has remained elusive, and thorough understanding of this process may highlight new opportunities for antiretroviral treatment strategies. In this study, we employed PALM and spt-PALM to investigate how HIV-1 assembly is spatially and temporally regulated through NC-vRNA interactions

at the plasma membrane. We should emphasize that the experiments were simplified to provide a generic landscape of the assembly process at the PM, and, as a result, some of the early assembly events occurring below the 20-nm length scale, including the formation of Gag assembly precursors (28) and the growth of these assembly precursors to a visualizable cluster, were not detected. Additionally, this study does not investigate how Gag assembly is mediated by cellular RNAs, which can also bind to Gag to form VLPs, particularly in the absence of vRNA (9–11). Nonetheless, our results should still be relevant to understanding the HIV-1 assembly process, as vRNA is the dominant RNA species that drives Gag assembly (5, 6, 34, 35).

Use of Modified Proviral Constructs for Studying Gag Assembly. One concern with imaging studies of HIV-1 assembly is possible interference with proper assembly of Gag into viral particles by fluorescent labels (36). To minimize potential interference, studies have employed cotransfection methods, in which fluorescent protein-tagged Gag and untagged Gag are expressed at different ratios between 1:1 and 1:10, with reported successful imaging of Gag assembly in the cellular context (16–23). Consistent with these findings, we showed that when mEOS2 was used as the reporter probe, cotransfection of the mEOS2-tagged construct and the untagged construct in a 1:4 ratio could yield expected particle assembly and vRNA packaging by Gag proteins and their NC mutants at the PM (Fig. 1 and *SI Appendix*, Figs. S2 and S3). Furthermore, while it is known that Gag can assemble into various dead-end structures that may not proceed to full virus formation (36, 37), the observed high level of colocalization (~90%) between Gag-mEOS2 and vRNA FISH signals at both the PM and in the supernatant observed in our study (Fig. 1 *B–E* and *SI Appendix*, Fig. S3 *B–E*) suggests that the majority of the mEOS2 signals detected at the PM reflect Gag complexes that resemble those within wild-type structures that can ultimately remodel into virus particles.

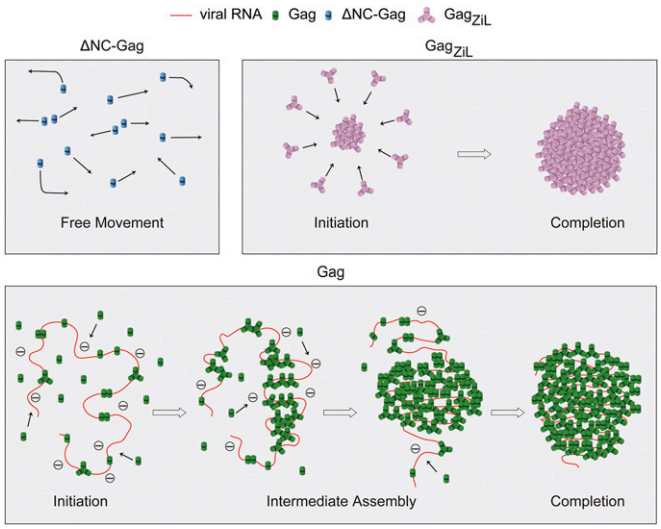

Fig. 4. Schematic model of how viral RNA promotes Gag assembly at the PM, based on PALM and spt-PALM analysis. Under conditions when Gag cannot cluster because the NC is deleted (ΔNC-Gag), Gag is highly dissociated and exhibits fast dynamic properties at the PM. When the NC is replaced with an isoleucine zipper to drive Gag trimerization independent of vRNA (Gag$_{ZiL}$), Gag forms tight clusters with slow dynamics. During wild-type viral formation, vRNA interacts with Gag molecules through nonspecific electrostatic interactions. With the dimer or trimer as the basic assembly unit, a tightly packed cluster could form until the electrostatic charge of the core is neutral. Thereafter, additional recruitment of Gag to the cluster slows, presumably as a result of increased electrostatic repulsion. This proceeds until the complex becomes fully assembled. vRNA mediates this process by tethering Gag molecules to prevent dissociation and high-density clustering and in so doing maintains the stability of the assembly environment.

Gag and NC Mutants Exhibit Different Nanoscale Organization at the PM: Implications for the Role of vRNA in Supporting Gag Assembly Architecture. PALM cluster analysis showed that Gag progresses through a series of intermediates before forming fully assembled complexes at the PM. This progression, rather than being a strictly monotonic process that favors dense packing of Gag molecules throughout its progression, as observed for Gag$_{ZiL}$, appears to be driven by at least two different mechanisms in sequence (Fig. 2 and *SI Appendix*, Fig. S5). Progression from small to midsize clusters involves extensive Gag clustering with increasing density, analogous to the behavior of Gag$_{ZiL}$. Further formation of larger clusters exhibits a different activity, with recruitment of more Gag molecules to the assembling clusters at a constant packing density. Because NC has multiple positively charged residues that are thought to interact with the negatively charged phosphate backbone of RNA, we suggest the observed nanoscale organization unique to Gag is a consequence of charge balance between NC and vRNA, which provides a large electrostatic surface for NC binding. During the initial phase, Gag molecules are highly attracted to vRNA, upon which they interact with assembly precursors, thought to contain a small number of Gag molecules, to form densely packed clusters until a critical cluster radius (~63 nm) is reached (*SI Appendix*, Fig. S5). Subsequently, the assembling clusters become less negatively charged and thus slow Gag accumulation, enabling stable constant-density growth of larger clusters.

Analysis of Lateral Diffusion Properties by spt-PALM Reveals Basic Gag Assembly Units as Low-Order Gag Multimers. Measurements of lateral diffusion through the use of single-molecule fluorescence microscopy can determine the stoichiometry of membrane-bound protein complexes in living cells (38). Since it has been hypothesized that vRNA promotes Gag assembly by inducing dimerization/trimerization of Gag molecules, we therefore tested whether diffusion properties observed using spt-PALM could elucidate the mechanism of Gag multimerization. Our results showed that ΔNC-Gag has a mean molecular diffusion coefficient ~3 times greater than that of Gag$_{ZiL}$ (Fig. 3*B*). As the molecular size of ΔNC-Gag (a monomer) is roughly one third that of the Gag$_{ZiL}$ trimer that is assumed to form (39), the observed diffusion coefficients suggest that diffusion of Gag mutants at the PM is governed by the Stokes–Einstein relation, as previously observed using engineered proteins harboring different numbers of the GRP1–pleckstrin homology domain on supported lipid bilayers (40). Therefore, as the mean diffusion coefficient of wild-type Gag was only slightly higher than Gag$_{ZiL}$ (Fig. 3*B*), this suggests that Gag diffuses at the PM through vRNA tethering in units of dimers or trimers, which serve as basic assembling units, as implicated in previous findings using biochemistry-based assays (14, 15). This close agreement in Gag stoichiometry between spt-PALM and previous biochemistry-based studies could lay the foundation for future studies that aim at studying the HIV-1 assembly process using fluorescence-imaging methods.

NC-vRNA Interactions Orchestrate Nanoscale Gag Assembly by Maintaining a Balance Between Gag Disassembly and High-Density Packing. The observed differences in nanoscale organizations, alongside the similarity of basic assembly units of Gag and Gag$_{ZiL}$, raise the possibility that vRNA has additional roles beyond merely driving the formation of basic Gag assembly units. Supporting this idea, analysis of directed-transport properties revealed significant differences in the lateral speed and acceleration between Gag and NC mutants (Fig. 3 *D* and *E*). Of the three proteins, ΔNC-Gag's lateral speed was the fastest,

accompanied by a positive acceleration. This suggests that the plasma membrane environment can exert forces to dissociate the ΔNC-Gag molecules from the assembly environment, resulting in their inability to cluster. Conversely, Gag_{ZiL} exhibited the lowest lateral speed with a negative acceleration. This is consistent with the tendency of Gag_{ZiL} to form high-density clusters and suggests these Gag_{ZiL} molecules undergo self-oligomerization in a manner that strongly inhibits Gag_{ZiL} migration out of the assembly environment. Finally, Gag lateral speed was intermediate to ΔNC-Gag and Gag_{ZiL}, with zero acceleration. Thus, it appears that the vRNA, which interacts with Gag but not ΔNC-Gag nor Gag_{ZiL}, promotes HIV-1 assembly by mediating a balance between external forces that drive Gag dissociation (as seen in the characteristics of ΔNC-Gag) and external forces that drive high-density packing (as seen in the characteristics of Gag_{ZiL}). Thus, in contrast to the notion that vRNA functions solely to drive Gag to form dimers/trimers and is dispensable for the subsequent assembly process, we suggest that vRNA is important for supporting and stabilizing assembly structures throughout the assembly process and does so by mediating a balance between external forces acting on the assembly environment.

Conclusion

Our results indicate that Gag nanoscale organization and dynamics at the PM are dependent on interactions with vRNA throughout the assembly process (Fig. 4). Without NC (ΔNC-Gag), the Gag protein freely migrates at the PM without clustering. When Gag molecules are able to form basic assembly units (trimers) independent of interaction with vRNA through replacement of NC with an isoleucine zipper (Gag_{ZiL}), Gag undergoes self-oligomerization to form high-density clusters that are highly immobile. Wild-type Gag interacts with vRNA to form clusters through a two-phase process, in which vRNA maintains the assembly environment by mediating a balance between forces that drive dispersion (as seen with ΔNC-Gag) and forces that drive high-density packing (as seen with Gag_{ZiL}). Thus, contrary to the hypothesis that vRNA only functions to drive formation of low-order Gag multimers, our results reveal crucial organizational and dynamic dependencies of the subsequent assembly process on NC-vRNA interactions. We propose that these dependencies could serve as a quality-control system to allow the virus to ensure that only properly assembled particles are produced and disseminated into the extracellular milieu. Moreover, given that cellular RNAs can also mediate Gag assembly, we envision the methodologies and findings described in the study could lay foundations for future studies, deepening our understanding of retroviral assembly and production.

Materials and Methods

We studied the bulk and nanoscale properties of Gag variants following procedures described previously (16, 19), with some modifications. Details are presented in *SI Appendix*.

ACKNOWLEDGMENTS. We thank Dr. Eric O. Freed (National Cancer Institute) and Dr. Prabuddha Sengupta (Janelia Research Campus) for providing useful comments. This project was supported by grants from the National Key R&D Program of China (2016YFA0501603 and 2016YFA0100702), the National Natural Science Foundation of China (31771583 and 81371613), and China's 1000 Young Talent Award program.

1. Aldovini A, Young RA (1990) Mutations of RNA and protein sequences involved in human immunodeficiency virus type 1 packaging result in production of noninfectious virus. *J Virol* 64:1920–1926.
2. Gorelick RJ, et al. (1990) Noninfectious human immunodeficiency virus type 1 mutants deficient in genomic RNA. *J Virol* 64:3207–3211.
3. Berkowitz RD, Luban J, Goff SP (1993) Specific binding of human immunodeficiency virus type 1 gag polyprotein and nucleocapsid protein to viral RNAs detected by RNA mobility shift assays. *J Virol* 67:7190–7200.
4. Kutluay SB, Bieniasz PD (2010) Analysis of the initiating events in HIV-1 particle assembly and genome packaging. *PLoS Pathog* 6:e1001200.
5. Comas-Garcia M, et al. (2017) Dissection of specific binding of HIV-1 Gag to the 'packaging signal' in viral RNA. *eLife* 6:e27055.
6. Dilley KA, et al. (2017) Interactions between HIV-1 Gag and viral RNA genome enhance virion assembly. *J Virol* 91:e02319-16.
7. Briggs JA, et al. (2004) The stoichiometry of Gag protein in HIV-1. *Nat Struct Mol Biol* 11:672–675.
8. Kutluay SB, et al. (2014) Global changes in the RNA binding specificity of HIV-1 gag regulate virion genesis. *Cell* 159:1096–1109.
9. Rulli SJ, Jr, et al. (2007) Selective and nonselective packaging of cellular RNAs in retrovirus particles. *J Virol* 81:6623–6631.
10. Muriaux D, Mirro J, Harvin D, Rein A (2001) RNA is a structural element in retrovirus particles. *Proc Natl Acad Sci USA* 98:5246–5251.
11. Comas-Garcia M, Davis SR, Rein A (2016) On the selective packaging of genomic RNA by HIV-1. *Viruses* 8:246.
12. Yu F, et al. (2001) Characterization of Rous sarcoma virus Gag particles assembled in vitro. *J Virol* 75:2753–2764.
13. Campbell S, Rein A (1999) In vitro assembly properties of human immunodeficiency virus type 1 Gag protein lacking the p6 domain. *J Virol* 73:2270–2279.
14. Crist RM, et al. (2009) Assembly properties of human immunodeficiency virus type 1 Gag-leucine zipper chimeras: Implications for retrovirus assembly. *J Virol* 83: 2216–2225.
15. Accola MA, Strack B, Göttlinger HG (2000) Efficient particle production by minimal Gag constructs which retain the carboxy-terminal domain of human immunodeficiency virus type 1 capsid-p2 and a late assembly domain. *J Virol* 74:5395–5402.
16. Qu N, et al. (2017) Inhibition of retroviral Gag assembly by non-silencing miRNAs promotes autophagic viral degradation. *Protein Cell*, 10.1007/s13238-017-0461-z.
17. Pak AJ, et al. (2017) Immature HIV-1 lattice assembly dynamics are regulated by scaffolding from nucleic acid and the plasma membrane. *Proc Natl Acad Sci USA* 114: E10056–E10065.
18. Chen J, et al. (2016) HIV-1 RNA genome dimerizes on the plasma membrane in the presence of Gag protein. *Proc Natl Acad Sci USA* 113:E201–E208.
19. Chen AK, et al. (2014) MicroRNA binding to the HIV-1 Gag protein inhibits Gag assembly and virus production. *Proc Natl Acad Sci USA* 111:E2676–E2683.
20. Jouvenet N, Simon SM, Bieniasz PD (2009) Imaging the interaction of HIV-1 genomes and Gag during assembly of individual viral particles. *Proc Natl Acad Sci USA* 106: 19114–19119.
21. Ivanchenko S, et al. (2009) Dynamics of HIV-1 assembly and release. *PLoS Pathog* 5: e1000652.
22. Jouvenet N, Bieniasz PD, Simon SM (2008) Imaging the biogenesis of individual HIV-1 virions in live cells. *Nature* 454:236–240.
23. Müller B, et al. (2004) Construction and characterization of a fluorescently labeled infectious human immunodeficiency virus type 1 derivative. *J Virol* 78:10803–10813.
24. Betzig E, et al. (2006) Imaging intracellular fluorescent proteins at nanometer resolution. *Science* 313:1642–1645.
25. Sengupta P, Van Engelenburg S, Lippincott-Schwartz J (2012) Visualizing cell structure and function with point-localization superresolution imaging. *Dev Cell* 23:1092–1102.
26. Manley S, et al. (2008) High-density mapping of single-molecule trajectories with photoactivated localization microscopy. *Nat Methods* 5:155–157.
27. Dawson L, Yu XF (1998) The role of nucleocapsid of HIV-1 in virus assembly. *Virology* 251:141–157.
28. Hendrix J, et al. (2015) Live-cell observation of cytosolic HIV-1 assembly onset reveals RNA-interacting Gag oligomers. *J Cell Biol* 210:629–646.
29. Dooher JE, Schneider BL, Reed JC, Lingappa JR (2007) Host ABCE1 is at plasma membrane HIV assembly sites and its dissociation from Gag is linked to subsequent events of virus production. *Traffic* 8:195–211.
30. Campbell S, Vogt VM (1995) Self-assembly in vitro of purified CA-NC proteins from Rous sarcoma virus and human immunodeficiency virus type 1. *J Virol* 69:6487–6497.
31. Notelaers K, et al. (2014) Analysis of alpha3 GlyR single particle tracking in the cell membrane. *Biochim Biophys Acta* 1843:544–553.
32. Wang D, et al. (2012) Forward transport of proteins in the plasma membrane of migrating cerebellar granule cells. *Proc Natl Acad Sci USA* 109:E3558–E3567.
33. Bouzigues C, Morel M, Triller A, Dahan M (2007) Asymmetric redistribution of GABA receptors during GABA gradient sensing by nerve growth cones analyzed by single quantum dot imaging. *Proc Natl Acad Sci USA* 104:11251–11256.
34. Chen J, et al. (2009) High efficiency of HIV-1 genomic RNA packaging and heterozygote formation revealed by single virion analysis. *Proc Natl Acad Sci USA* 106: 13535–13540.
35. Liu Y, et al. (2017) HIV-1 sequence necessary and sufficient to package non-viral RNAs into HIV-1 particles. *J Mol Biol* 429:2542–2555.
36. Larson DR, Johnson MC, Webb WW, Vogt VM (2005) Visualization of retrovirus budding with correlated light and electron microscopy. *Proc Natl Acad Sci USA* 102: 15453–15458.
37. Carlson LA, et al. (2010) Cryo electron tomography of native HIV-1 budding sites. *PLoS Pathog* 6:e1001173.
38. Aggarwal V, Ha T (2016) Single-molecule fluorescence microscopy of native macromolecular complexes. *Curr Opin Struct Biol* 41:225–232.
39. Zhang Y, Qian H, Love Z, Barklis E (1998) Analysis of the assembly function of the human immunodeficiency virus type 1 gag protein nucleocapsid domain. *J Virol* 72: 1782–1789.
40. Knight JD, Lerner MG, Marcano-Velázquez JG, Pastor RW, Falke JJ (2010) Single molecule diffusion of membrane-bound proteins: Window into lipid contacts and bilayer dynamics. *Biophys J* 99:2879–2887.